Seventh South African Conference on Computational and Applied Mechanics
SACAM10
Pretoria, 10−13 January 2010


# EXPERIMENTAL INVESTIGATION INTO THE UNSTEADY EFFECTS ON NON-AXISYMMETRIC TURBINE ENDWALL CONTOURING

**Dwain Dunn** [*,1], **Glen Snedden**[*,2] **and Theodor W von Backström**[†]

[*] Aeronautical Systems
DPSS
CSIR, PO Box 395, Pretoria, 0001, South Africa,
[1]ddunn@csir.co.za, [2]gsnedden@csir.co.za.

[†]Department of Mechanical and Mechatronic Engineering
University of Stellenbosch, Private Bag X1, Matieland 7602, South Africa
twvb@sun.ac.za.

**Keywords:** Non-axisymmetric endwalls, secondary flow, unsteady effects

## Abstract

Turbine manufacturers are striving to develop turbines that are more efficient. One area of focus has been the control of secondary flows through the use of non-axisymmetric endwalls. The majority of development has been performed in cascades or by using computational fluid dynamics.

The current investigation was carried out on a $1^1/_2$ stage low pressure turbine. The performance of a generic endwall profile was tested using 2 component hot-film anemometry. The generic endwall of Durham University was chosen for analysis

It has been shown that the contouring improved the performance of the turbine. Detailed analysis showed that the improved performance was due to a reduction in the rotor exit secondary velocity. The deviation of the rotor exit yaw angle from the design rotor exit yaw angle was reduced.

Furthermore it was found that the passage vortex of the contoured rotor was not as tightly wrapped around the horse shoe vorticies as the annular rotor passage vortex. Due to the passage vortex being more unwrapped in the contoured case, the tip leakage flow was drawn towards the hub more. The spanwise extent of the tip leakage flows was increased, but the magnitude was reduced.

## 1 Introduction

With the price of oil steadily increasing, turbine manufacturers are striving to improve efficiency. One of the methods used for this is to improve the power to weight ratio, by reducing the weight of the turbine, but maintain the specific thrust. This is usually done by increasing the blade loading,hich increases the impact of the secondary flows on the turbine efficiency.

**Nomeclature**

| | |
|---|---|
| $\alpha$ | Yaw angle ($^\circ$) |
| $C$ | Velocity ($m/s$) |
| CFD | Computational Fluid Dynamics |
| $\eta$ | Isentropic efficiency ($\%$) |
| $f$ | Frequency |
| $FFT$ | Fast Fourier Transform |
| PLA | Phase locked average |
| $S$ | Span ($mm$) |
| $v$ | Velocity ($m/s$) |
| $y^+$ | Near wall Reynolds Number |

Subscripts:

| | |
|---|---|
| 1 | Stator inlet |
| 3 | Rotor outlet |
| $s$ | Sample |
| $sec$ | Secondary component |
| $Stage$ | From stator inlet to downstream rotor outlet |
| $t$ | Tangential |
| T | Total |
| $x$ | Axial |

Historically three sources of loss have been considered in turbines, namely: profile loss, leakage loss and endwall loss. Denton [1] stated that approximately one third of the endwall loss in high pressure turbines can be attributed to entropy generation in the annular boundary layer upstream, within and downstream of the blade row. A second component is caused by the mixing loss of the inlet boundary layer which gets amplified by the secondary flow. Secondary kinetic energy is the third component which makes up approximately a $^1/_4$ of the total loss.

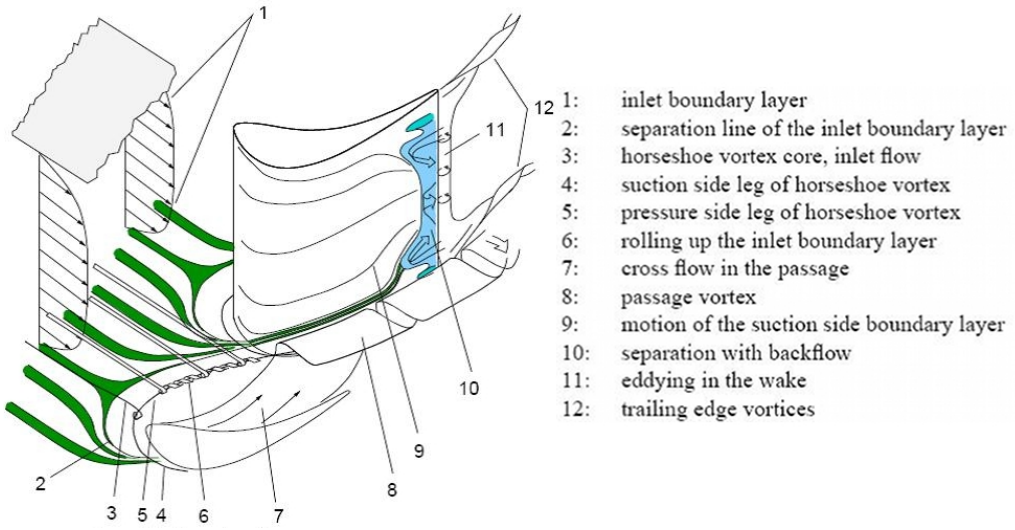


**Figure 1:** Schematic showing the various vortical structures in a turbine reproduced from Eymann *et al.* [2] who reproduced it from Vogt and Zippel [3].

A schematic of the secondary flow structure can be seen in Figure 1. Hawthorne [4] was the

**Table 1:** Experimental instrumentation used for the unsteady flow mapping

| Unsteady Instrumentation | | |
|---|---|---|
| Unsteady Flow mapping | TSI 1240-20 / 1247A-10 X-probe (film) | $\pm 0.77\%$ mean velocity<br>$\pm 6\%$ of variance |
| Turbulence | TSI 1211-20 single component film | $\pm 0.77\%$ mean velocity |
| Tangential Traverse | Custom cable system | Better than $0.01^\circ$ |
| Radial and Yaw traverse | Rotadata Mini actuator | $0.01$mm<br>$0.1^\circ$ |

first to describe the secondary flow vortex system. It has been shown that the passage vortex (numbered 8 in Figure 1) is the dominant flow feature, and has been reported by numerous researchers [5, 6, 7, 8].

One of the methods currently being investigated to control secondary flows is through endwall contouring [9]. The aim of non-axisymmetric endwall contouring is to control the cross passage flow to reduce the secondary flows. Currently most of the research in secondary flows are performed in stationary, $2D$ linear cascades. Cascades however reduce complexities thus making it easier to isolate certain effects for investigation.

Snedden *et al.* [10] investigated the generic linear cascade P2 endwall of Ingram [9, 11] in a rotating turbine test rig. It was found that the generic endwalls did improve the turbine efficiency, however there was room for improvement by customising the endwall for a rotating environment.

Snedden *et al.* [10] performed steady state experiments using a five hole probe. The current investigation was aimed at investigating the effects of the endwall in the unsteady time frame using a hot film probe.

## 2 Experimental setup

The test rig that was used can be described as being a low pressure $1^1/_2$ stage turbine. As shown in Figure 2, the turbine rig's axis was vertical. A compressor was used below the turbine to draw the air in through the bell mouth at the inlet resulting in clean inlet flow. The instrumentation used on the turbine test rig was described by Snedden *et al.* [12], the unsteady instrumentation is listed in Table 1 .

A generic contour for the endwall similar to that used by Ingram [9] at Durham University was chosen for the current investigation. The blades used were based on those of Ingram [9] in order to line up with the endwall. The blades used by Ingram [9] however were prismatic blades typically used for cascades. Thus the blades had to be changed to take into account the rotational effects caused by a rotating environment. The resulting blades with the annular endwall and the contoured endwall can be seen in Figure 3.

The design summary for the blades can be seen in Table 2. The difference in inlet and outlet angle from hub to casing takes rotation into account, since at the casing, the blade travels faster then it does at the hub.

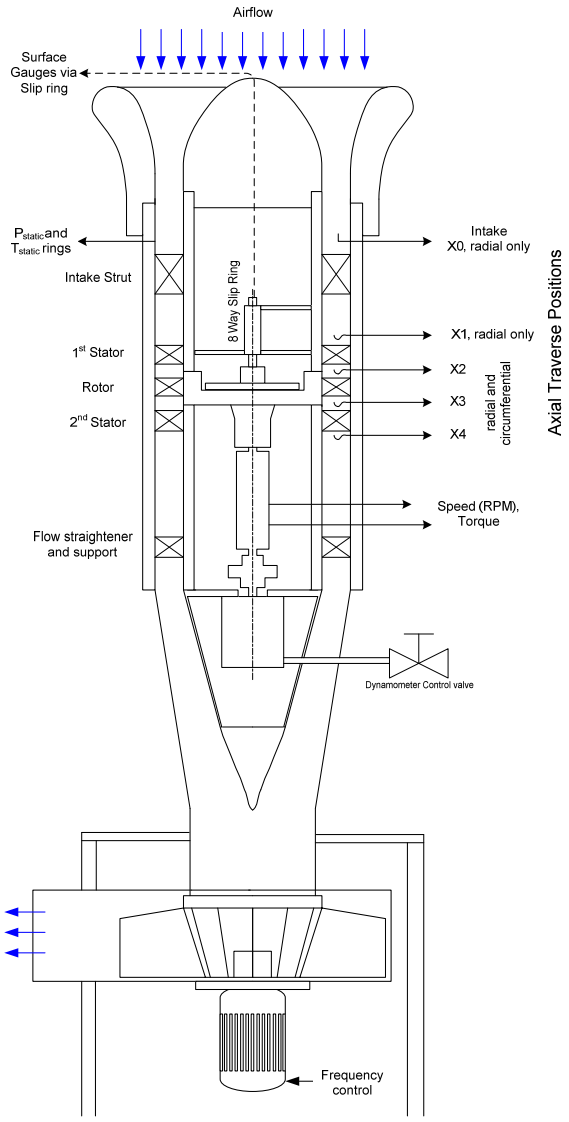


**Figure 2:** Schematic of the turbine rig

## 3 Measurement and analysis technique

The hot-film probes were calibrated using the TSI model $1129$ auto-calibrator, using the TSI prescribed technique [14]. King's Law was used for the calibration curve, as it consistently had the lowest mean squared error.

A grid of $15$ radial points and $23$ tangential points was chosen for the sampling, producing $345$ measurement points. The tangential points were set at $1^{\circ}$ apart whereas the radial points were $4mm$ apart. At each point $64$ thousand samples were collected at $f_s = 100kHz$. The high number of blade passings per location allows for phase lock averaging (PLA) to be performed using the additional samples. PLA is the process whereby several samples are averaged such that the phase is the same [15]. PLA aids with removing of noise from a discretely sampled data.

A step function was sampled in conjunction to the hot film probe that produced a $5V$ drop at the

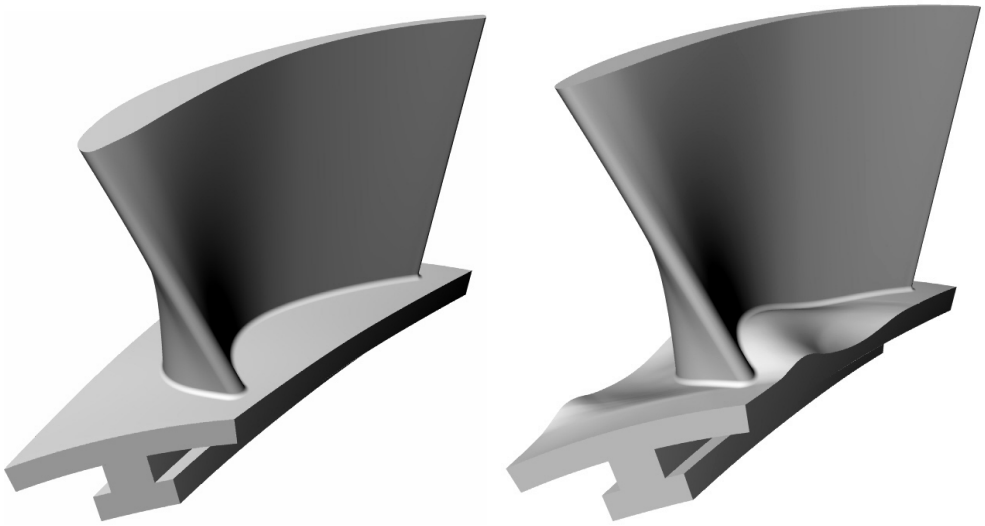

(a) Annular endwall (b) Contoured endwall

**Figure 3:** CAD representation of the rotor blades to be tested

**Table 2:** Test rig design summary

| | | |
|---|---|---|
| **Inlet** | | |
| Axial Velocity | | $21.38m/s$ |
| **1st Stator** | | |
| No. of Blades | | 30 |
| Inlet Angle | Hub | $0°$ |
| | Casing | $0°$ |
| Outlet Angle | Hub | $68.26°$ |
| | Casing | $61.20°$ |
| Midspan Outlet | Absolute Velocity | $46.4m/s$ |
| **Rotor** | | |
| No. of Blades | | 20 |
| Rotational Speed | | $2300RPM$ |
| Inlet Angle | Hub | $42.75°$ |
| | Casing | $-23.98°$ |
| Outlet Angle | Hub | $-68.00°$ |
| | Casing | $-71.15°$ |
| Midspan Outlet | Relative Velocity | $57.4m/s$ |
| Modified Stage Power[a] | | $3.42kW$ |
| Stage Pressure Ratio | | 1.0393 |

[a]Rotor outlet angle adjusted according to [13]

exact same rotor angle per revolution. The step function gives an indication of the rotor phase angle. Using the first rise of step function allowed the data to be aligned with respect to the rotor passings. The data is averaged over a complete revolution, or 20 blade passings using the step function mentioned. A $FFT$ of the sample data, and the step function are used to select the most frequent number of samples/frequency per complete revolution. It is these samples

that are averaged, allowing the largest number of data sets to be averaged. Slight changes in rotor speed are removed by using only the data that produces the same number of samples per revolution. On average in excess of $8$ revolutions are used per point for the PLA.

The data was then decimated such that there were the same numbers of samples for each grid location. This was done by applying a spline locally to the data, and resampling at the required time intervals. All the samples for all grid locations were then at the same time interval.

The decimated data was then time averaged and radially averaged to produce velocity profiles. The hot-film probe used however is only capable of $2D$ measurements, perpendicular to the probe, i.e. axial and tangential velocities. Thus velocity magnitudes were calculated using only the axial and tangential velocity components.

## 4 Results

**Table 3:** Stage total-to-total efficiency comparison

| | Annular | Non-axisymmetric | $\Delta$ |
|---|---|---|---|
| Steady experiment | 77.0 | 77.4 | 0.4 |

Table 3 was taken from Snedden *et al.* [10]. It shows that the contoured rotor does improve efficiency. Even though the improvement was small, it still exceeded experimental uncertainty. Due to the nature of the unsteady experimentation, unsteady efficiencies could not be calculated since only velocities were available and not temperature or pressure.

The graphs in Figure 4 to Figure 9 were time averaged. These graphs give an indication of the scatter in the data due to the unsteadiness, i.e. all the data measured will fall between the maximum and the minimum values regardless of the sample time.

One of the most notable features of the profiles presented was the large tip leakage flows. From approximately $65\%$ span to the casing at $100\%$ span. The large tip leakage flow was due to the large tip gap of $1.7\%$ span. The access hole used to insert the hot-film probe would also affect the flow. Since this investigation was aimed at endwall flow it was felt that this did not adversely effect the results. The contoured rotor did however exhibit an increase in the tip leakage flow compared to the annular endwall.

One of the biggest changes between the contoured and annular case can be seen in the magnitude of the peak velocity between $15\%$ and $25\%$ span in Figure 4. The magnitude of the axial velocity was reduced by approximately $5m/s$, making the outlet velocity profile more uniform. The vortex core at $25\%$ span was not only reduced, but the maximum fluctuation (between maxmimum value and minimum value) was also reduced. The maximum velocity was thus found in the tip leakage flow region, and not the passage vortex system as with the annular case. A uniform outlet velocity is favourable since the downstream blade rows will have a more uniform and clean inlet flow.

With respect to Figure 6, it was evident that the contouring produced a more uniform outlet velocity. The region below approximately $70\%$ span for the annular case had a range larger than that seen in the contoured case. It can also be seen that the tip leakage region characteristic has been changed, as mentioned in the the steady state investigations of Snedden *et al.* [10].

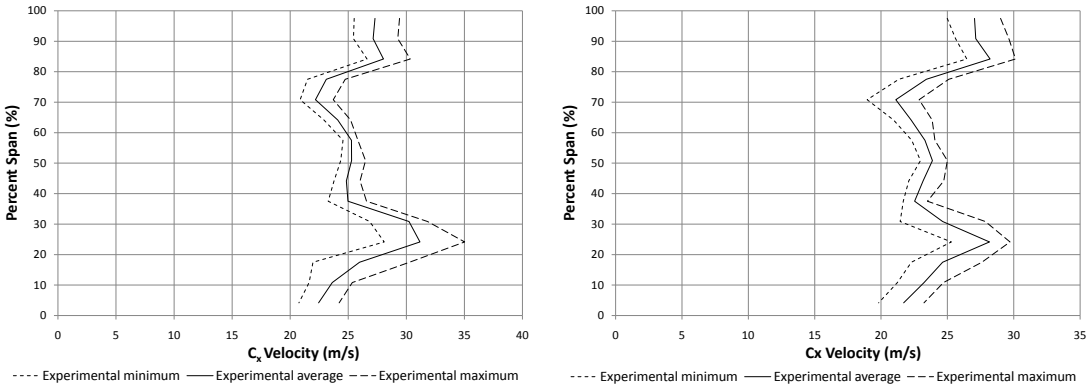


(a) Annular Endwall (b) Contoured Endwall

**Figure 4:** Comparison of the rotor exit axial velocity

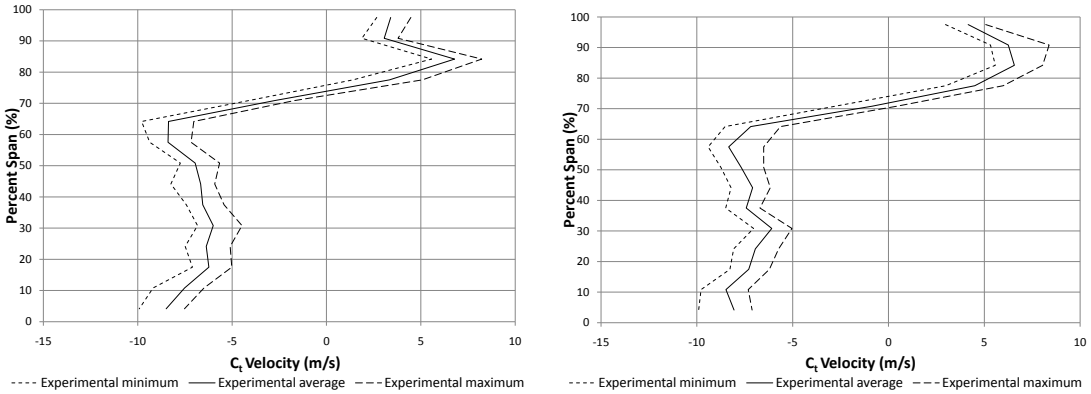


(a) Annular Endwall (b) Contoured Endwall

**Figure 5:** Comparison of the rotor exit tangential velocity

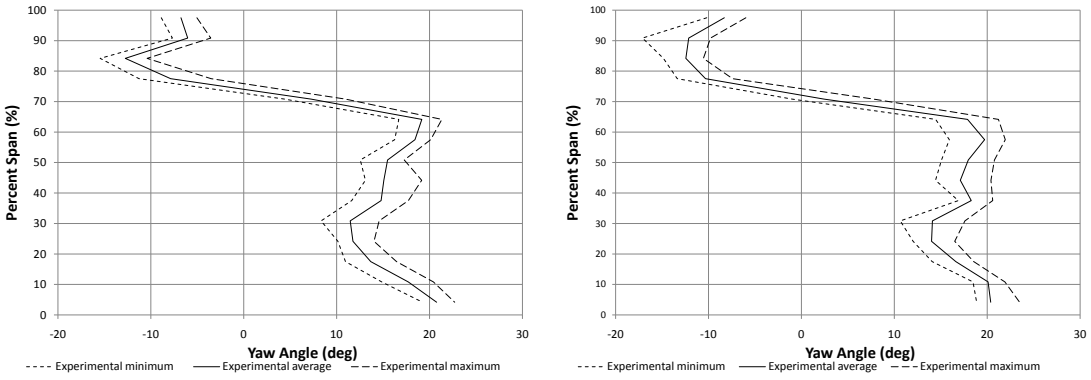


(a) Annular Endwall (b) Contoured Endwall

**Figure 6:** Comparison of the rotor exit flow yaw angle

The mechanism that caused this is not fully understood, but investigations are continuing.

Figure 7 and 8 show the instantaneous yaw contour plots. Looking at the passage vortex core at approximately $25\%$ span it can be seen that the endwall contouring has reduced the intensity

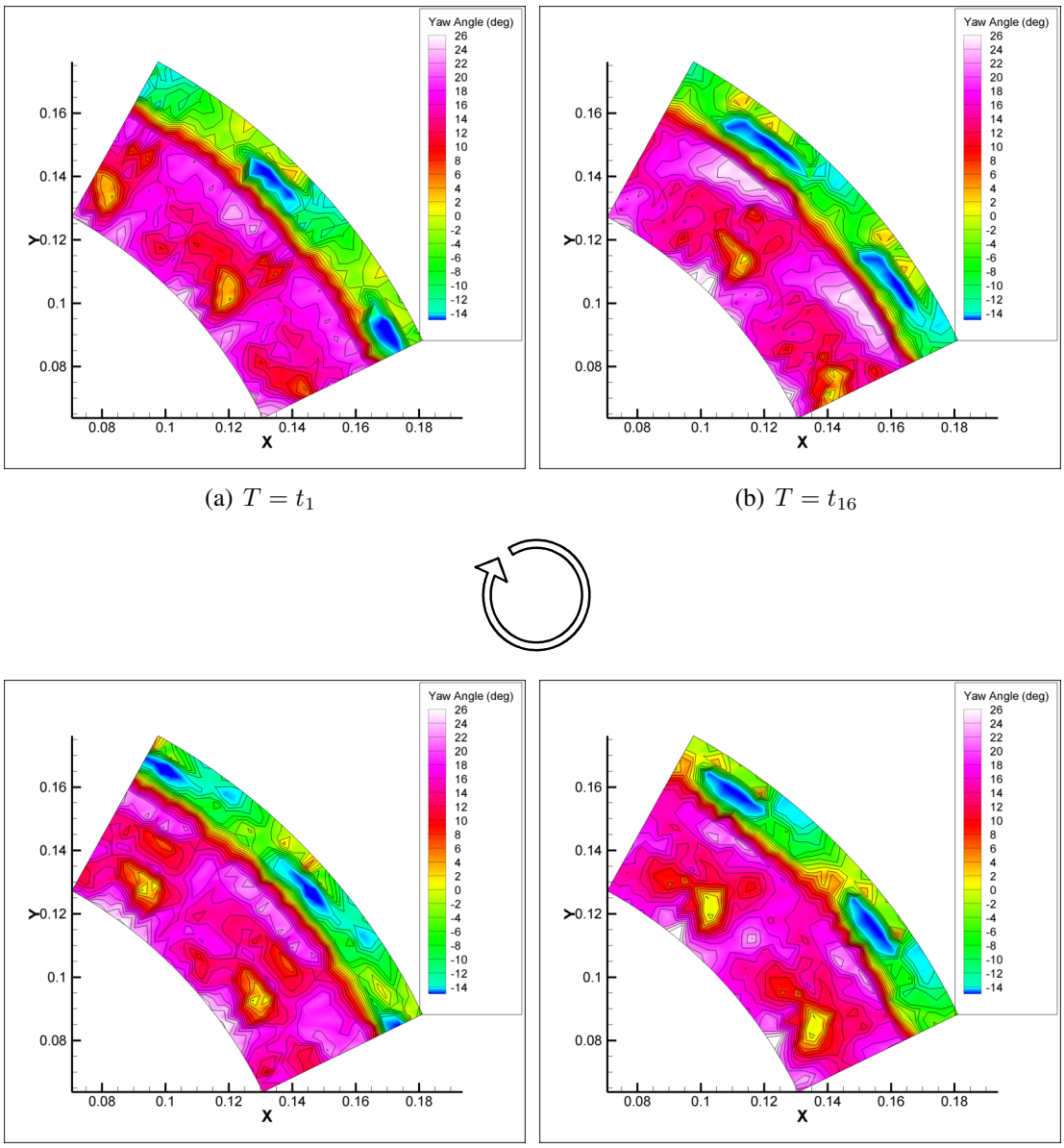


(a) $T = t_1$ (b) $T = t_{16}$

(d) $T = t_{46}$ (e) $T = t_{31}$

**Figure 7:** Annular endwall: Contours of yaw angle

of the secondary flow vortex core. The vortex has been reduced in the tangential direction, but moved slightly higher in the spanwise direction. The result of this can be seen by the increased tip leakage flow. The passage flow can also be seen to be more uniform for the contoured rotor.

The effect of the contouring becomes more evident when looking at the secondary velocity plots in Figure 9. Secondary velocity was calculated using the method of Matsunuma [16]:

$$v_{sec} = \frac{\bar{v} \times sin(\alpha - \bar{\alpha})}{v_{mean}} \tag{1}$$

Where $\bar{v}$ is the velocity magnitude, in this case the magnitude of the radial and tangential velocity, $\alpha$ is the absolute yaw angle, $\bar{\alpha}$ is the average absolute yaw angle and $v_{mean}$ is the

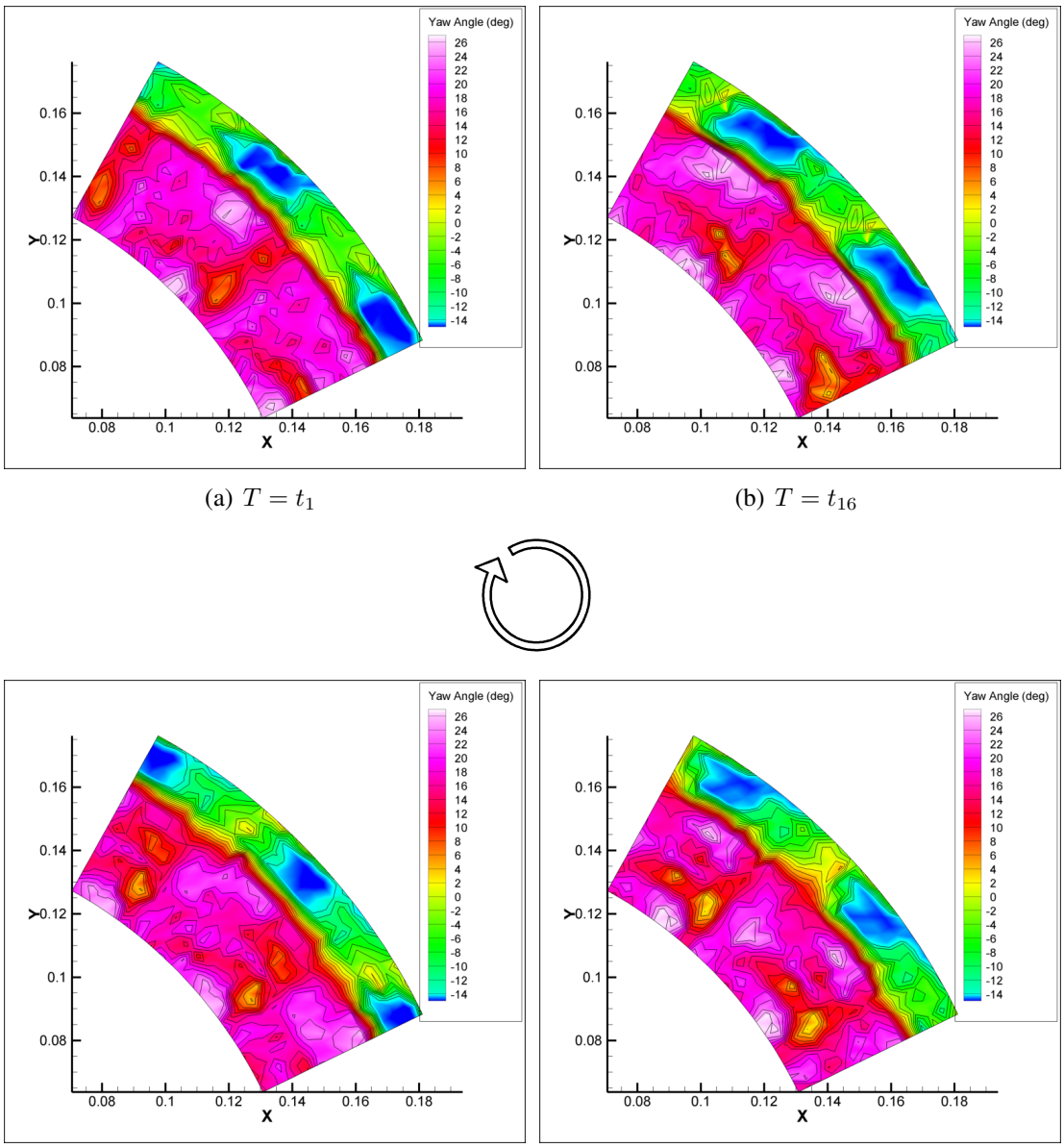


(a) $T = t_1$ (b) $T = t_{16}$

(d) $T = t_{46}$ (e) $T = t_{31}$

**Figure 8:** Contoured endwall: Contours of yaw angle

mean value of the velocity magnitude.

At $90\%$ span and over the magnitude of the secondary velocity was greatly increased with the addition of the endwall contouring, as mentioned previously. At the hub however the magnitude was reduced. The maximum range of the secondary velocity was also reduced below $60\%$ span for the contoured cases. The reduction in secondary velocities was found to correspond to an increase in efficiencies.

## 5 Conclusion and recommendations

Contouring has been shown to improve the isentropic stage total-to-total efficiency. Specifically when investigating the flow field it was found that the contoured endwall had the following

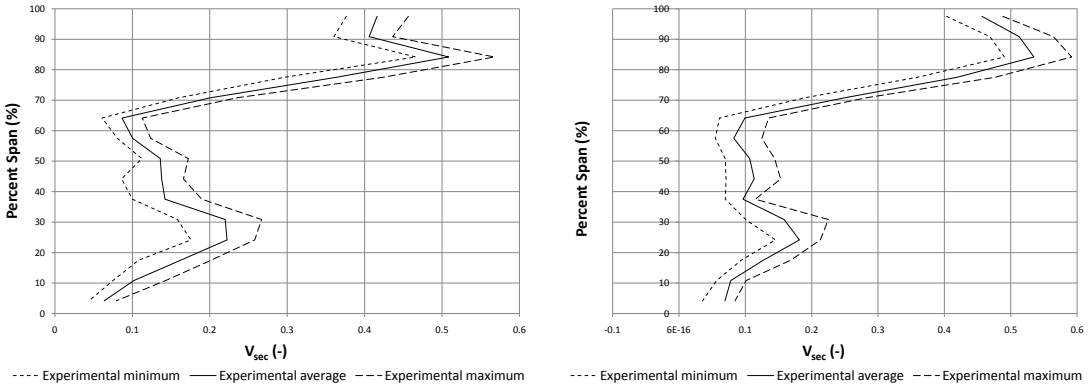


(a) Annular Endwall (b) Contoured Endwall

**Figure 9:** Comparison of the rotor exit secondary velocity

effects on the rotor exit flow:

- Isentropic total-to-total efficiency was improved.
- The tip leakage flows were increased in intensity and size.
- The vortex core was reduced in strength by approximately $5m/s$, and the fluctuations due to the blade passings were reduced.
- The rotor exit flow was more uniform in direction as well as magnitude.
- The secondary velocities have been reduced and magnitudes were more consistent.

Even though non-axisymmetric endwall contouring has shown to improve the efficiency, it should be noted that the endwall was designed for use in a linear cascade. Snedden *et al.* [10] states that the efficiency could be improved more with an endwall that is specifically designed for the turbine.

## 6 Acknowledgments

VITAL is a new collaborative research project, running for six years, which aims to significantly reduce aircraft engine noise and $CO_2$ emissions. It has a total budget of 91 million euros, including 51 million euros in funding from the European Commission. Snecma leads a consortium of 53 partners gathering all major European engine manufacturers: Rolls-Royce Plc, MTU Aero Engines, Avio, Volvo Aero, Techspace Aero Rolls-Royce Deutschland and ITP, and the airframer Airbus.

The work in this paper above has been performed under SP6/WP6.2.10 - Unsteady endwall contouring and AVIO specifically contributed to the work presented in the paper.

## References

[1] JD Denton. Loss mechanisms in turbomachines. In *ASME Gas Turbine Congress*, pages 1–40. Scholars Paper, 1993.

[2] S Eymann, U Reinmoller, R Niehuis, W Forster, Beversdorff M, and J Gier. Improving 3d flow characteristics in a multistage lp turbine by means of endwall contouring and airfoil design modification - part 1: Design and experimental investigation. pages –. ASME TURBO EXPO GT-2002-30352, 2002.

[3] H.F. Vogt and M. Zippel. Sekundarstromungen in turbinengittern mit geraden und gekrummten schaufeln; visualisierung im ebenen wasserkanal. *Forschung im Ingenieurwesen, Engineering Research*, 62 no. 9:247 – 253, 1996.

[4] W.R. Hawthorne. Rotational flow through cascades. *Journal of Mechanical and Applied Mathematics*, 3, 1955.

[5] P Marchal and CH Sieverding. Secondary flows within turbomachine bladings. In *Secondary flows in turbomachines*, volume AGARD-CP-214 Paper 11, pages –. 1977.

[6] SH Moustapha, GJ Paron, and JHT Wade. Secondary flows in cascades of highly loaded turbine blades. *Transactions of ASME Journal of Engineering for Gas Turbines and Power*, 107:1031–1038, 1985.

[7] HP Hodson and RG Dominy. Three-dimensional flow in a low pressure turbine cascade at its design condition. *Transaction of the ASME Journal of Turbomachinery*, 109:177–185, 1987.

[8] S Harrison. Secondary loss generation in a linear cascade of high-turning turbine blades. *Transactions of ASME Journal of Turbomachinery*, 112:618–624, 1990.

[9] GL Ingram. *Endwall Profiling for the Reduction of Secondary Flow in Turbines*. PhD thesis, University of Durham, July 2003.

[10] Glen Snedden, Dwain I. Dunn, Grant L. Ingram, and David G. Gregory-Smith. The application of non-axisymmetric endwall contouring in a single stage, rotating turbine. In *ASME Turbo Expo*, number GT2009-59169, 2009.

[11] G Ingram, D Gregory-Smith, and N Harvey. Experimental quantification of the benefits of end-wall profiling in a turbine cascade. pages –. ISABE 2003-1101, 2003.

[12] Glen Snedden, Thomas Roos, Dwain Dunn, and David Gregory-Smith. Characterisation of a refurbished 1 stage turbine test rig for flowfield mapping behind blading with non-axisymmetric contoured endwalls. In *ISABE*, number ISABE 2007-1363, 2007.

[13] HIH Saravanamuttoo, H Cohen, and GFC Rogers. *Gas Turbine theory*. Pearson Education Limited, 5th edition, 2001.

[14] TSI Incorporated. *Model 1129 automated air velocity calibrator: Instruction Manual*. TSI Incorporated, 500 Cardigan Road, St. Paul MN 55164, revision b edition, July 2003.

[15] Barry S. Perlman and Victor H. Auerbach. A phase-locking technique for estimating the ensemble average of time-series data. volume ASSP-25, pages 295–299. IEEE Transactions on Acoustics, Speech and Signal Processing, 1977.

[16] T Matsunuma. Unsteady flowfield of an axial-flow turbine rotor at a low reynolds number. In *ASME Turbo Expo 2006: Power for Land Sea and Air*, pages –. ASME GT2006-90013, may 2006.